Short- and Medium-Range Order in Sodium Aluminophosphate Glasses: New Insights from High-Resolution Dipolar Solid-State NMR Spectroscopy

Long Zhang and Hellmut Eckert*

Institut für Physikalische Chemie, Westfälische Wilhelms-Universität Münster, Corrensstr. 30, D-48149 Münster, Germany

Received: January 24, 2006; In Final Form: March 22, 2006

The structures of sodium aluminophosphate glasses prepared by both sol−gel as well as melt-cooling routes have been extensively characterized by high-resolution solid-state ^{23}Na, ^{27}Al, and ^{31}P single and double-resonance NMR techniques, including quantitative connectivity studies by ^{27}Al ↔ ^{31}P and ^{23}Na ↔ ^{31}P rotational echo double-resonance (REDOR) methods. Studies along four compositional lines, I: $(AlPO_4)_x-(NaPO_3)_{1-x}$, II: $(Na_2O)_x-(AlPO_4)_{1-x}$, III: $(NaAlO_2)_x-(NaPO_3)_{1-x}$, and IV: $(Al_2O_3)_x(NaPO_3)_{1-x}$, reveal that the network structures of those glasses that are accessible by either preparation method are essentially identical. However, the significantly extended glass-forming ranges available by the sol−gel route facilitate exploration of the structure/composition relationships in more detail, revealing a number of interesting universal features throughout the whole glass system. Both short- and medium-range order appear to be controlled strongly by the O/P ratio of the glasses studied: Up to an O/P ratio of 3.5 (pyrophosphate composition), aluminum is predominantly six-coordinated and fully connected to phosphorus ($Al(OP)_6$ sites). In the region $3.5 \leq O/P \leq 4.0$, a dramatic structural transformation takes place, leading to the appearance of additional four- and five-coordinated aluminum species whose second coordination spheres are also entirely dominated by phosphorus. The structure of glasses with an O/P ratio of precisely 4.0 (orthophosphate) is dominated by $Al(OP)_4$ units. As the O/P ratio increases beyond 4.0, the average extent of Al−O−P connectivity is decreased significantly. Here, new types of five- and six-coordinated aluminum units, which are only weakly connected to phosphorus, are formed, while the network modifier is attracted mainly by the phosphate units.

1. Introduction

The potential of phosphate glasses for a variety of technologically important applications has been limited by their generally low physical and chemical stability. The addition of alumina into phosphate glasses has long been known to improve these characteristics remarkably, resulting, for example, in drastically increased water resistance.[1,2] Thus, an understanding of the basic structural changes that occur with the addition of alumina is important for the rational design of new glasses for specific applications. Using standard melt-cooling techniques, the reported glass-forming region in the $Na_2O-Al_2O_3-P_2O_5$ glass system is relatively small and the maximum Al_2O_3 content is limited to about 25 mol %.[2,3] We reported previously that the glass-forming range in the $Na_2O-Al_2O_3-P_2O_5$ system can be extended significantly via the sol−gel preparation route,[4,5] making it possible to study compositional control of glass structure more comprehensively and in greater detail.

Solid-state nuclear magnetic resonance (NMR) techniques have provided some of the most powerful characterization tools for disordered materials because of their well-proven ability to provide a wealth of local structural information.[6−8] A number of insightful NMR investigations of aluminophosphate glass systems have already been published,[4,5,9−16] focusing mainly on local structural aspects probed by ^{27}Al and ^{31}P magic-angle spinning (MAS) NMR. Recently, several MAS-based NMR techniques have been developed that utilize through-space internuclear dipole−dipole coupling to probe structural connectivity and spatial proximity. Among these techniques, rotational echo double resonance (REDOR)[17−19] and rotational echo adiabatic passage double resonance (REAPDOR)[20,21] have proven to be enormously powerful in characterizing multispin dipolar interactions in disordered systems involving quadrupolar nuclei.[22−24] Using such techniques, we have recently been able to provide detailed quantitative information concerning (a) network-former connectivities, (b) spatial correlations between network former and network modifier and, (c) the atomic distribution of the network modifying ions themselves in a variety of binary and ternary glass systems.[8] In this contribution, we investigate these issues for the sodium aluminophosphate glass system over a greatly extended compositional range afforded by sol−gel preparation routes. On the basis of the detailed quantitative dipole−dipole coupling information obtained, we present a comprehensive structural model for sodium aluminophosphate glasses.

2. NMR Methodology

The experimental strategy used in the present manuscript includes the quantitative analysis of high-resolution ^{23}Na, ^{27}Al, and ^{31}P NMR solid-state NMR spectra, afforded by single-pulse MAS and (in the case of the quadrupolar nuclei ^{23}Na and ^{27}Al) also triple-quantum (TQ)-MAS NMR to separate chemical shift from nuclear electric quadrupole coupling information. Furthermore, a key part of this study is based on the quantitative analysis of internuclear magnetic dipole−dipole interactions. To this end, we have previously developed the rotational echo double resonance (REDOR) technique into an experimental tool

* Corresponding author. Tel: 0049-251-8329161. Fax: 0049-251-8329159. E-mail: eckerth@uni-muenster.de.

10.1021/jp060501s CCC: $33.50
Published on Web 04/20/2006

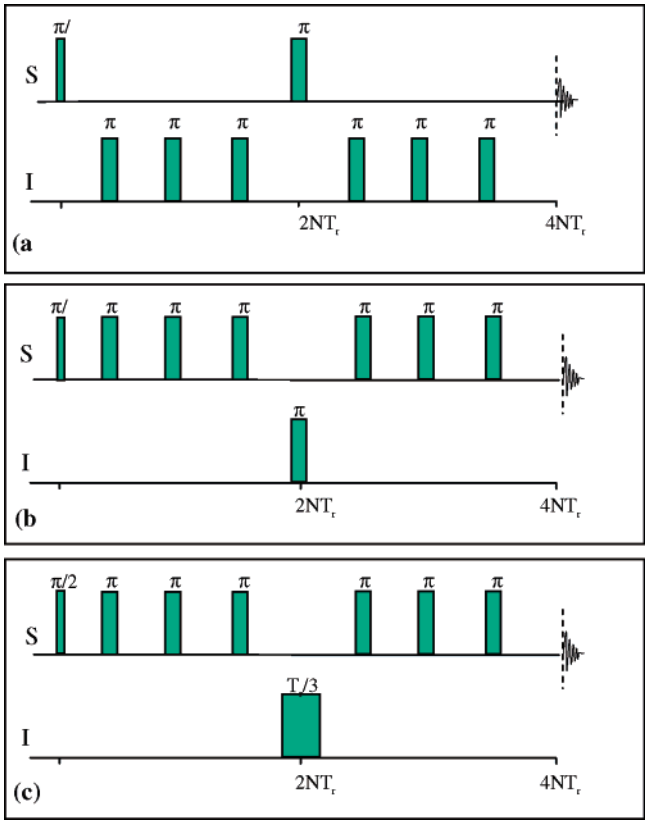

Figure 1. NMR pulse sequences used in the present study. (a) Sequence used for ^{27}Al{^{31}P} and ^{23}Na{^{31}P} REDOR; (b) sequence used for ^{31}P{^{23}Na} REDOR; (c) sequence used for ^{31}P{^{27}Al}REAPDOR. In all cases, dipolar recoupling is accomplished by the π (adiabatic) rf pulse of nonobserved nuclei in the middle of the rotor period.

for site-resolved heteronuclear dipolar coupling measurements in glasses.[8,19,23−25] Figure 1 shows the two S{I} REDOR pulse sequences used in the present study.[17−19] A normalized difference signal $\Delta S/S_0 = (S_0 - S)/S_0$ is measured in the absence (intensity S_0) and the presence (intensity S) of the dipolar interactions of the observed nuclei S with the second nuclear species I. Determination of $\Delta S/S_0$ under systematic variation of the number of rotor cycles N yields the so-called REDOR curve, in which the data are plotted as a function of dipolar evolution time NT_r (T_r being the duration of one rotor period). For isolated spin-$^1/_2$ pairs these curves possess a universal shape, allowing the straightforward determination of the magnetic dipole−dipole coupling constant.[26,27] In contrast, the analysis of S{I} REDOR curves in inorganic glasses is complicated by multispin interactions, distance distributions, and interference by nuclear electric quadrupolar couplings. We have shown previously that the problem can be simplified by confining the REDOR data analysis to the initial curvature, where $\Delta S/S_0 \leq 0.2$.[19,22,28] In this limit of short dipolar evolution times, the REDOR curve is found to be independent of specific spin system geometries, and can be approximated by a simple parabola:

$$\frac{\Delta S}{S_0} = \frac{4}{3\pi^2} M_2^{SI} (NT_r)^2 \qquad (1)$$

The curvature of this parabola is closely related to the van-Vleck second moment $M_2^{SI} = M_2(S\{I\})$, a quantity that can be used to characterize average dipole−dipole coupling strengths also in those cases for which the order and geometry of the spin systems is unknown and possibly ill-defined. In cases where the dipolar dephasing of the observed spins occurs in the local field of $I > {}^1/_2$ nuclei such as ^{23}Na ($I = {}^3/_2$) several additional complications enter. First of all, the different possible Zeeman states m_I for the I nuclei differ in the respective sizes of their z components and hence generate dipolar fields of different magnitudes at the observed spins.[29,30] Second, for strong nuclear electric quadrupolar coupling, the anisotropic broadening of the $|^1/_2> \leftrightarrow |^3/_2>$ "satellite transitions" produces large resonance offsets, which reduce the efficiency of π pulses in causing population inversion. In the limit of very large first-order quadrupolar splitting (rf nutation frequency $\nu_1 \ll C_Q$, the quadrupolar coupling constant), pulses applied to the I nuclei in the REDOR sequences will affect only the central $|^1/_2> \leftrightarrow |-^1/_2>$ coherences. In this regime only those S spins that are coupled to I nuclei in Zeeman states with $|m_I| = {}^1/_2$ are expected to yield a REDOR response. Detailed simulations of this situation have led to the conclusion that it is desirable in such cases to minimize the number of π pulses applied to the quadrupolar nuclei, making the REDOR sequence of Figure 1b the method of choice. As we have shown previously, the initial curvature analysis discussed above can be extended to systems containing $I = {}^3/_2$ nuclei by using the expression

$$\frac{\Delta S}{S_0} = \frac{1}{15\pi^2} (2 + 18 f_1) M_2^{SI} (NT_r)^2 \qquad (2)$$

where the efficiency factor f_1 ($0 \leq f_1 \leq 1$) accounts for the extent to which the dipolar coupling of S spins to I spins in their outer Zeeman states still influences the REDOR response. Again, eq 2 is valid for the initial regime ($0 \leq \Delta S/S_0 \leq 0.2$) only.[22]

The whole data analysis procedure can thus be summarized as follows: On the basis of the nuclear electric quadrupolar coupling Hamiltonion parameters determined experimentally, a universal REDOR curve is computed (using the SIMPSON code[31]) using explicitly those experimental conditions under which the REDOR data were taken. This simulation curve is fitted to a parabola (eq 2), resulting in the appropriate f_1 value, which is then applicable for the analysis of the experimental data set. Using the f_1 value determined in this fashion, the experimental data are fitted to eq 2, resulting in an experimental second moment. This value can then be compared with calculations based on structural models using the well-known van Vleck equation[32]

$$M_2^{SI} = \left(\frac{\mu_0}{4\pi}\right)^2 \frac{4}{15} I(I+1) \hbar^2 \gamma_S^2 \gamma_I^2 \sum_S r_{IS}^{-6} \qquad (3)$$

where γ_I and γ_S are the gyromagnetic ratios of the nuclei I and S involved, and r_{IS} are the internuclear distances. In the present study, we will use this approach to analyze the dipolar field created by ^{23}Na at the observed ^{31}P nuclei.

The sequence of Figure 1b is just a special case of the more general REAPDOR (rotational echo adiabatic passage double resonance) experiment (Figure 1c) in which the central pulse applied in the middle of the dipolar evolution period creates adiabatic mixing of the various I-Zeeman states under the influence of MAS. In the case of REAPDOR, the optimum pulse-length for generating a maximum difference signal amounts to one-third of the rotor period.[33] In the present application, REAPDOR is used for qualitative studies of the local dipolar fields created by the spin-$^5/_2$ ^{27}Al nuclei at the ^{31}P sites.

3. Experimental Section

3.1. Sample Preparation and Characterization. All of the glass samples were prepared through an aqueous sol−gel route

TABLE 1: Experimental Conditions Used in the Double-Resonance NMR Experiments

combination	^{23}Na{^{31}P}	^{27}Al{^{31}P}	^{31}P{^{23}Na}	^{31}P{^{27}Al}
expt	REDOR		REDOR	REAPDOR
ν_r (kHz)[a]	10−15		10−15	12−14
$\tau_{90°}$(S) (μs)[b]	3.0	3.0	4.0	4.0
$\tau_{90°}$(I) (μs)[c]	4.0	4.0	3.0	4.0
τ_a (μs)[d]				22

[a] MAS rotor frequency. [b] S-spin-90° pulse length. [c] I-spin-90° pulse length. [d] Adiabatic passage time in REAPDOR.

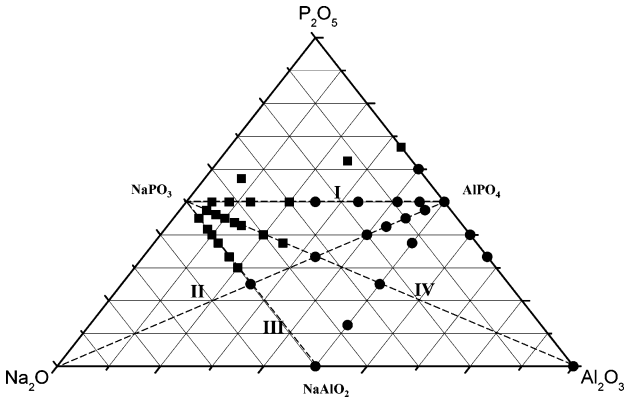

Figure 2. Ternary phase diagram showing the four composition lines investigated, and the compositions (mol %) of the glass samples prepared by the sol−gel route. Circles indicate glasses, which are not accessible via melt-cooling.

described previously,[4,5] using aluminum lactate, NaH_2PO_4 (or H_3PO_4 or $NaPO_3$), and sodium acetate as precursors. For comparison with the glasses made by the sol−gel route, sodium aluminophosphate bulk glasses were also prepared by the conventional melt-quenching method. To this end, 30-g batches of Al_2O_3 (>99%, Fluka), $NaPO_3$ (95−97%, Fluka), P_2O_5 (99%, Fluka), and Na_2CO_3 (99%, Fluka) were melted in a Pt crucible within a Nabertherm Supertherm furnance (HFL16/17) for 1−2 h at ∼1100−1600 °C (depending on the compositions), using procedures reported previously.[2,4] The glass melts were cast into a cold steel mold and then annealed for 1 h near the glass transition temperature, T_g. The glassy state was verified by X-ray powder diffraction (Guinier method) on all of the samples prior to NMR study, and T_g values were measured by differential thermal analysis (DTA) using a NETZSCH STA409 thermal analyzer at a heating rate of 10 K/min.

3.2. NMR Studies. All of the NMR measurements were carried out on Bruker DSX-400 and DSX-500 spectrometers equipped with 4-mm single- and double-resonance NMR probes at magic angle spinning (MAS) rotation frequencies of 10−15 kHz. At the magnetic field strengths of 9.4 T (11.7 T), the resonance frequencies were, respectively, 105.9 MHz (132.2 MHz) for ^{23}Na, 104.3 MHz (130.3 MHz) for ^{27}Al, and 160.4 MHz (202.5 MHz) for ^{31}P. Typical acquisition parameters for single-pulse measurements were: pulse length 5.0 μs (90° flip angle) for ^{31}P and 1.0 μs (30° solid flip angle) for both ^{27}Al and ^{23}Na, and recycle delays 90 s for ^{31}P and 0.5 s for both ^{27}Al and ^{23}Na. The ^{23}Na, ^{27}Al, and ^{31}P NMR chemical shifts are referenced to 1 M NaCl aqueous solution, 1 M $Al(NO)_3$ aqueous solution and 85% H_3PO_4, respectively. Average ^{23}Na ($I = 3/2$) and ^{27}Al ($I = 5/2$) quadrupolar coupling and isotropic chemical shift parameters were measured by two-dimensional triple-quantum (TQ)-MAS NMR,[34−36] employing the three-pulse zero-quantum filtering variant[35,36] at spinning speeds of 12−15 kHz. The rf field strengths of the first two hard pulses and the third soft pulse corresponded to nutation frequencies of

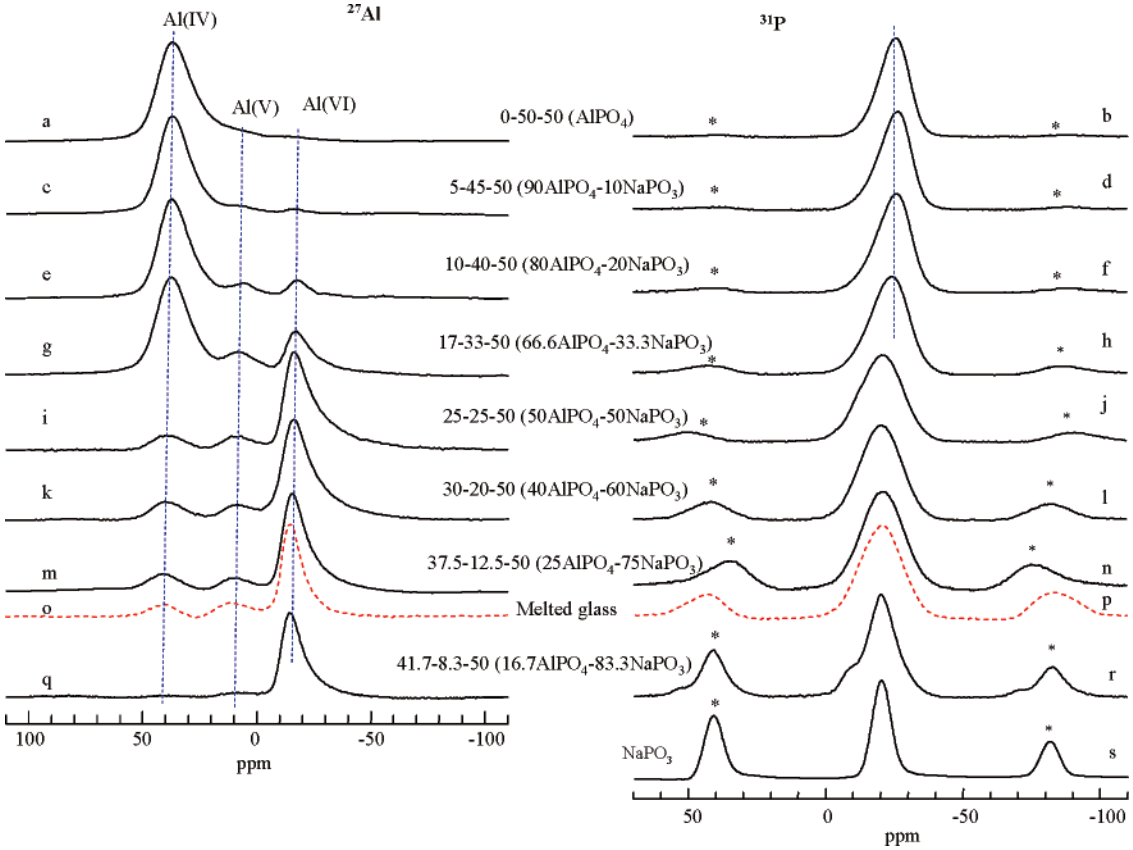

Figure 3. ^{27}Al (left) and ^{31}P (right) MAS NMR spectra of $AlPO_4$−$NaPO_3$ glasses derived from a sol−gel route. Spinning sidebands are indicated with asterisks. Dashed curves indicate spectra of melt-cooled glasses.

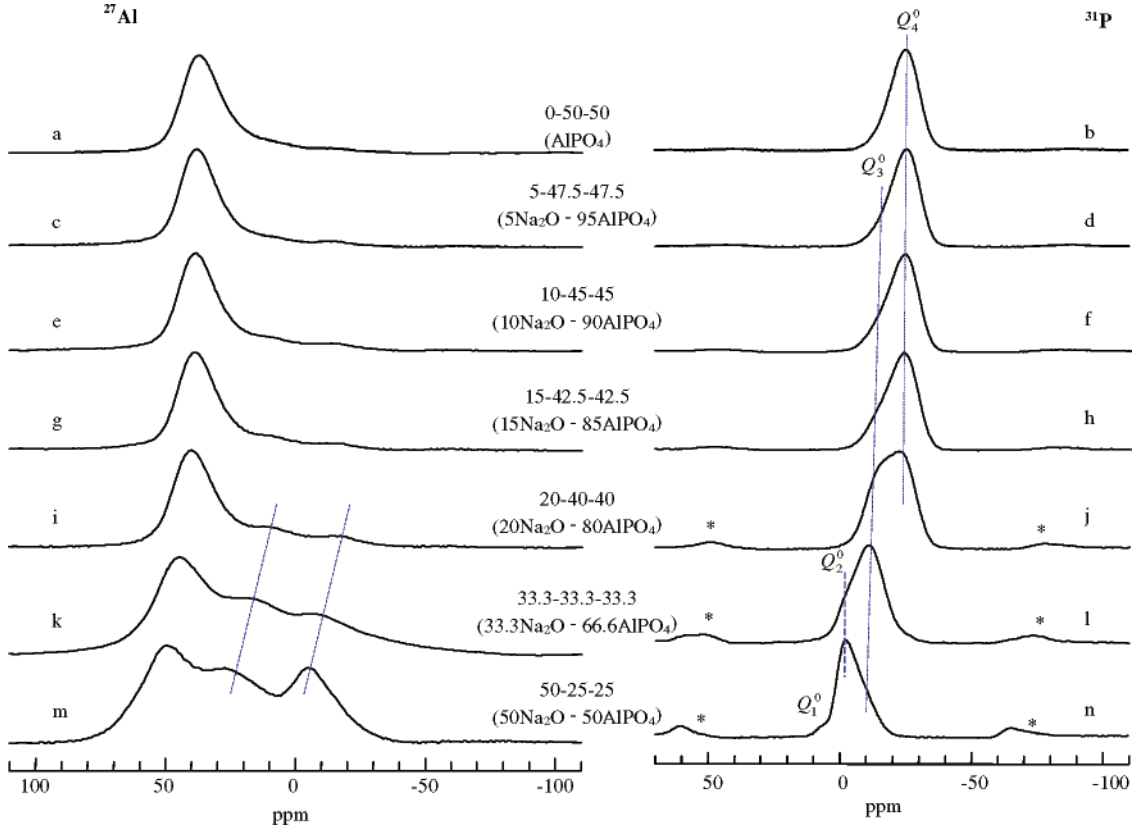

Figure 4. 104.3 MHz ^{27}Al (left) and 162.4 MHz ^{31}P (right) MAS NMR spectra of $Na_2O-AlPO_4$ glasses derived from a sol−gel route. Spinning sidebands are indicated with asterisks.

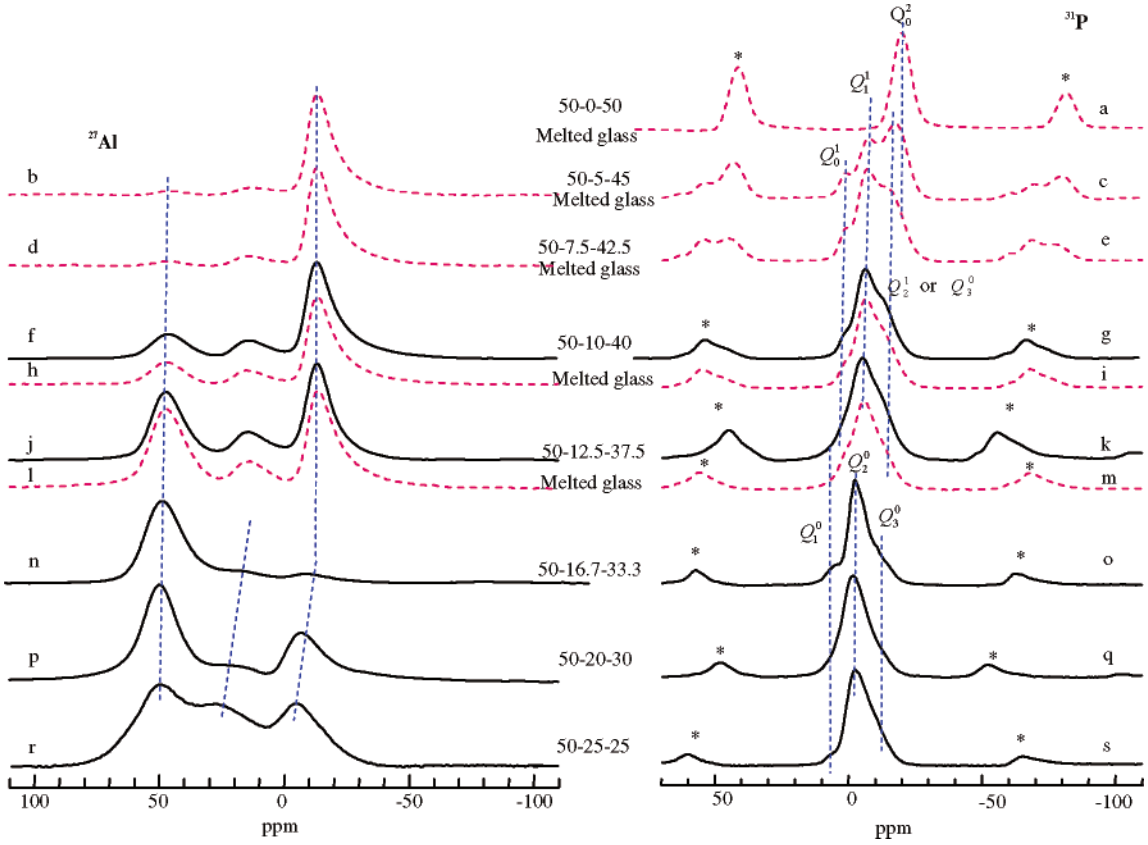

Figure 5. ^{27}Al (left) and MHz ^{31}P (right) MAS NMR spectra of $NaAlO_2-NaPO_3$ glasses derived from a sol−gel route. Spinning sidebands are indicated with asterisks. Dashed curves indicate spectra of melt-cooled glasses.

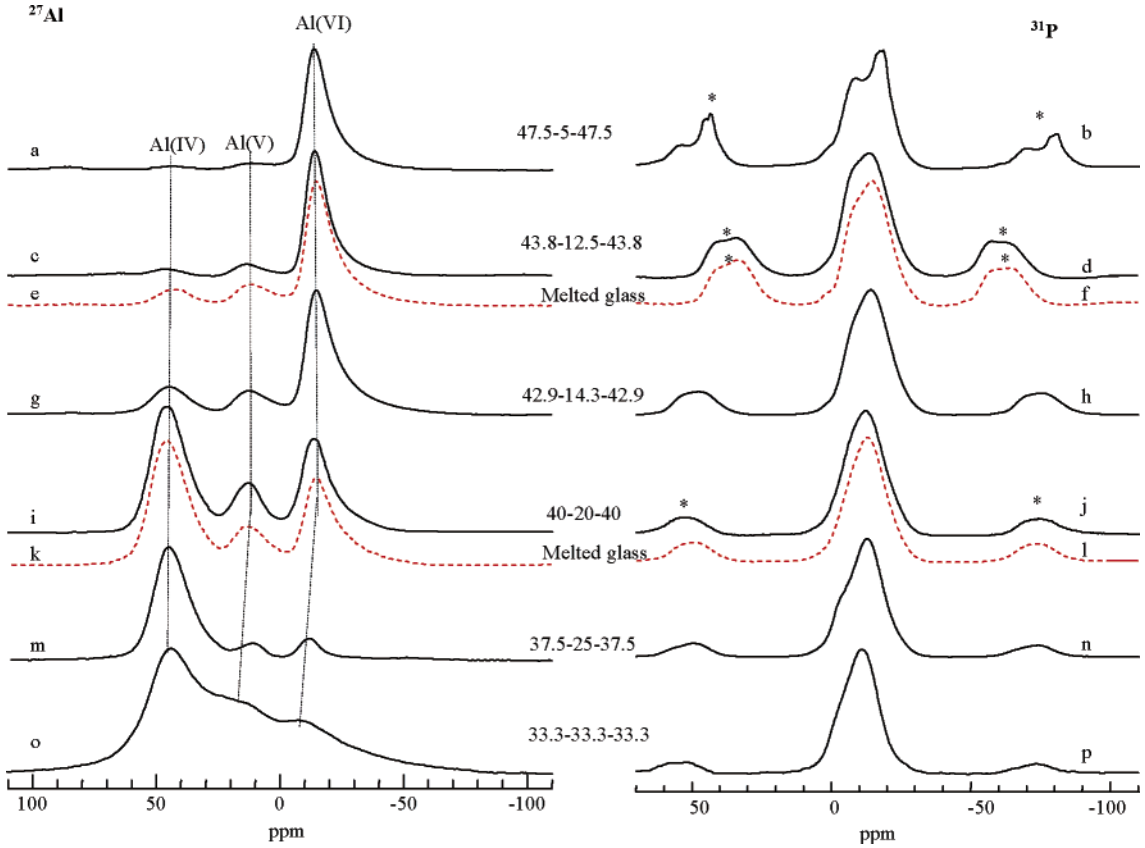

Figure 6. ^{27}Al (left) and ^{31}P (right) MAS NMR spectra of $Al_2O_3-NaPO_3$ glasses derived from a sol−gel route. Spinning sidebands are indicated with asterisks. Dashed curves indicate spectra of melt-cooled glasses.

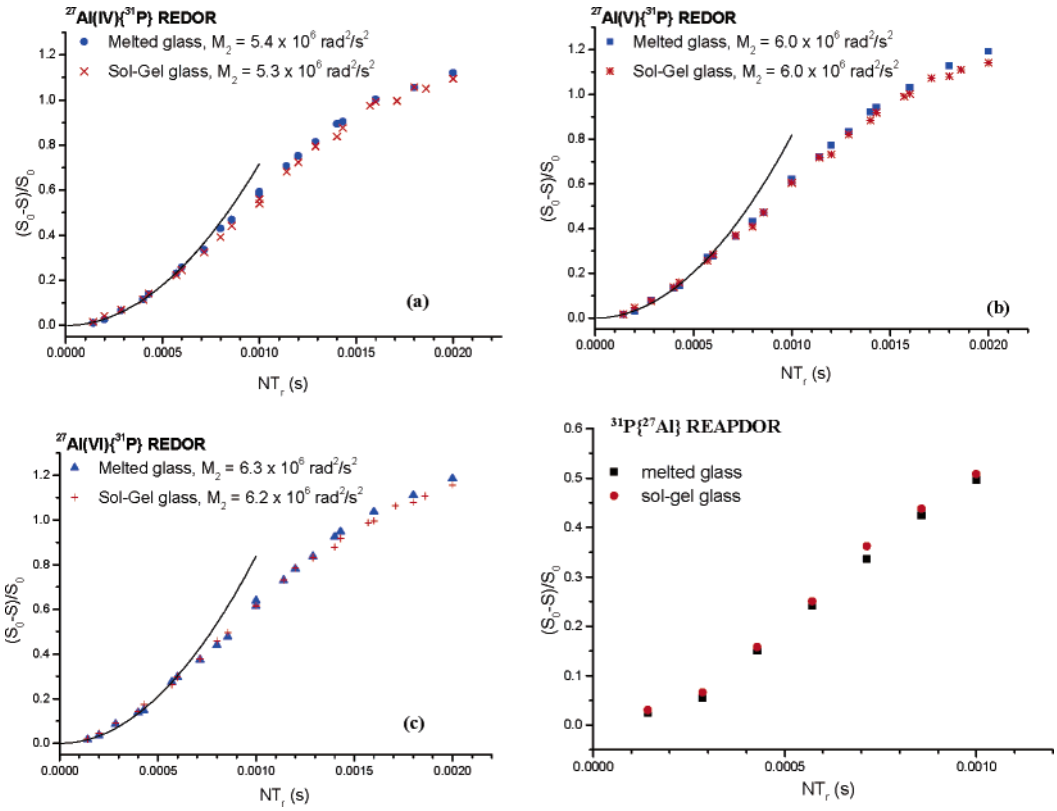

Figure 7. ^{27}Al ↔ ^{31}P dipolar dephasing curve of {50−12.5−37.5} glasses, prepared via sol−gel route and melt-cooling method. (a) ^{27}Al(IV){^{31}P} REDOR; (b) ^{27}Al(V){^{31}P} REDOR; (c) ^{27}Al(VI){^{31}P} REDOR; (d) ^{31}P{^{27}Al} REAPDOR showing the average extent of dipolar coupling of phosphorus by aluminum in both glasses.

TABLE 2: ^{27}Al and ^{31}P Isotropic Chemical Shifts (δ_{cs}), Nuclear Electric Quadrupolar Coupling Parameters, P_Q,[a] Relative Peak Area (*RA*) and ^{31}P − ^{27}Al Dipolar Second Moments $M_2(^{27}Al\{^{31}P\})$ for Sodium Aluminophosphate Glasses, Prepared via Both Sol−Gel and Melt-Cooling Routes[b]

		Al(IV)					Al(V)				Al(VI)			
glass composition $Na_2O-Al_2O_3-P_2O_5$		$\delta(^{31}P)$[c]/ ppm	δ_{cs}/ ppm	P_Q/ MHz	*RA*	M_2/ 10^6rad^2/s^2	δ_{cs}/ ppm	P_Q/ MHz	*RA*	M_2/ 10^6rad^2/s^2	δ_{cs}/ ppm	P_Q/ MHz	*RA*	M_2/ 10^6rad^2/s^2
I. $AlPO_4-NaPO_3$														
50−0−50	M	−20.1												
41.7−8.3−50	S	−19.4	48.2	3.7	0.04	nm	17.8	3.7	0.05	nm	−10.7	2.9	0.91	nm
37.5−12.5−50	S	−20.2	47.3	3.7	0.11	5.2	17.1	3.6	0.1	6.3	−10.5	2.8	0.79	6.2
	M	−20.4	48.1	3.8	0.08	5.4	17.5	3.7	0.1	6.1	−10.2	3.0	0.72	6.3
30−20−50	S	−20.1	46.9	3.6	0.12	nm	16.5	3.5	0.11	nm	−10.6	3.0	0.77	nm
25−25−50	S	−19.9	46.4	3.5	0.17	5.3	15.2	3.4	0.15	6.1	−11.2	2.9	0.68	6.2
17−33−50	S	−23.0	44.8	3.7	0.61	5.3	14.9	3.6	0.13	6.0	−10.4	2.9	0.26	6.3
10−40−50	S	−24.6	44.2	3.4	0.84	5.4	14.5	3.3	0.08	6.2	−10.7	2.8	0.08	6.2
5−45−50	S	−25.0	44.0	3.4	0.93	nm	14.4	3.5	0.05	nm	−10.3	3.0	0.02	nm
0−50−50	S	−25.9	43.7	3.2	0.91	5.6	-	-	0.03	-			0.04	
II. $Na_2O-AlPO_4$														
0−50−50	S	−25.9	43.7	3.2	0.91	5.6			0.03	-			0.04	-
5−47.5−47.5	S	−24.5	45.2	3.3	0.81	nm	18.2	3.5	0.07	nm	−7.1	3.1	0.04	nm
10−45−45	S	−23.8	46.6	3.1	0.82	5.4	19.8	3.7	0.12		−6.4	3.3	0.06	-
15−42.5−42.5	S	−23.3	47.2	3.4	0.8	5.4	21.3	3.6	0.15		−5.6	3.4	0.05	-
20−40−40	S	−20.2	47.8	3.2	0.72	nm	22.6	3.7	0.18	nm	−5.4	3.2	0.09	nm
33−33−33	S	−10.2	51.2	3.3	0.55	5.2	24.5	3.5	0.23	4.3	−4.8	3.0	0.22	3.4
50−25−25	S	−4.2	58.6	4.4	0.41	4.6	30.3	3.9	0.28	1.8	0.2	3.2	0.31	2.7
III. $NaAlO_2-NaPO_3$														
50−0−50	M	−20.1												
50−5−45	M	−12.3	53.0	3.4	0.06		20.8	3.9	0.07		−9.9	3.0	0.87	6.3
50−7.5−42.5	M	−10.4	53.1	3.6	0.07	5.5	20.9	3.8	0.08	6.2	−9.5	3.1	0.85	6.3
50−10−40	S	−8.6	53.5	3.7	0.25	nm	21.2	3.8	0.17	nm	−9.4	3.3	0.58	nm
	M	−8.5	53.4	3.5	0.23	5.2	21.0	3.6	0.15	6.1	−9.4	3.4	0.62	6.4
50−12.5−37.5	S	−6.7	53.4	3.5	0.41	5.3	21.1	3.9	0.15	6.0	−9.0	3.3	0.44	6.3
	M	−6.5	53.7	3.4	0.43	5.4	21.7	3.7	0.12	6.0	−8.8	3.4	0.45	6.2
50−16.7−33.4	S	−3.4	53.9	3.6	0.82	nm	19.9	3.8	0.10	nm	−6.8	3.1	0.08	nm
50−20−30	S	−3.1	54.6	3.8	0.69	5.1	24.6	3.9	0.08	3.7	−4.7	3.2	0.23	3.8
50−25−25	S	−4.2	58.6	4.4	0.41	4.6	30.3	3.9	0.28	1.8	0.2	3.2	0.31	2.7
IV. $Al_2O_3-NaPO_3$														
50−0−50	M	−20.1												
47.5−5−47.5	S	−15.1	48.1	3.7	0.04		18.1	3.7	0.06		−10.1	2.8	0.90	6.2
43.8−12.5−43.8	S	−11.2	51.0	3.8	0.09	5.3	19.0	3.7	0.13	6.0	−10.3	2.9	0.78	6.1
	M	−11.7	50.8	3.7	0.11	5.1	19.5	3.7	0.14	6.2	−10.2	3.0	0.75	6.4
43.9−14.3−43.9	S	−12.7	50.9	3.8	0.2	5.3	19.2	3.8	0.14	6.0	−10.7	2.9	0.65	6.3
40−20−40	S	−12.5	50.1	3.9	0.51	5.2	19.1	3.9	0.16	5.9	−10.5	2.8	0.33	6.2
	M	−12.8	49.7	3.7	0.49	5.3	18.7	3.9	0.15	6.1	−11.2	2.9	0.36	6.2
37.5−25−37.5	S	−11.1	50.4	3.5	0.78	5.3	16.2	3.7	0.1	5.1	−7.2	2.9	0.12	4.9
33−33−33	S	−10.2	51.2	3.3	0.51	5.2	24.5	3.5	0.23	4.3	−4.8	3.0	0.25	3.4

[a] Defined as $C_Q(1 + \eta^2/3)^{1/2}$. [b] The errors for parameters δ_{cs}, P_Q, and *RA* were less than ±0.3 ppm, ±0.1 MHz, and ±2%. Typical errors for the M_2 values are ±10%. [c] Chemical shift given by the center of gravity; S (M) − glasses prepared via sol−gel (melt-cooling) route; nm − not measured

approximately 130 and 6 kHz (^{27}Al), and 100 and 9 kHz (^{23}Na) respectively, for nonselective excitation on a liquid sample. Typically, 360 (for ^{27}Al) or 240 (for ^{23}Na) transients were accumulated for each t_1 increment, and a total of 240 increments were done at steps of 20 μs. The sheared spectra were analyzed by projecting the 2D contours for each individual site onto the F_1 and F_2 axes.[35,36]

All of the heteronuclear solid-state dipolar NMR studies were carried out on a Bruker DSX-500 spectrometer, using a 4-mm double-resonance probe. ^{27}Al{^{31}P} and ^{23}Na{^{31}P} REDOR experiments were measured with the pulse sequence of Figure 1a. To correct for the effect of experimental imperfections, the REDOR compensation scheme described in ref 28 was used. ^{31}P{^{23}Na} REDOR measurements were conducted with the pulse sequence of Figure 1b. The π pulses on the ^{31}P channel in both types of REDOR experiments were phase cycled according to the XY-4 scheme.[18] ^{31}P{^{27}Al} REAPDOR measurements were performed using the pulse sequence of Figure 1c. Table 1 gives a summary of the various double resonance experiments carried out and the specific conditions used. To increase the number of data points in the $0 \leq \Delta S/S_0 \leq 0.2$ analysis regime, some REDOR curves were measured at two or three different spinning speeds.

4. Results, Data Analysis, and Interpretation

Figure 2 summarizes the glass compositions investigated in the present study. Our results reveal that the glass-forming region in this system can be extended significantly by sol−gel preparation. Figures 3−6 summarize the ^{27}Al and ^{31}P MAS NMR spectra of all sol−gel derived sodium aluminophosphate glasses, representing the four compositional lines. The corresponding NMR spectra of some representative melt-prepared glasses with the same compositions are included (dashed curves). As indicated from Figure 3m−p, Figure 5f−m, Figure 6c−f and i−l, the spectra are almost identical for glasses prepared by both sol−gel and melt-cooling routes at any given composition, for which glasses can be prepared by both procedures. The structural similarity between both types of glasses is further

TABLE 3: ^{31}P Isotropic Chemical Shifts (δ_{cs}), Assignments (Q^0_{mAl}, $m = 0-4$), Relative Areas (RA), $M_2(^{31}P\{^{23}Na\})$ Values Measured for the Resolvable Signal Components in $(Na_2O)_x(AlPO_4)_{1-x}$ Glasses[a]

	Q^0_{1Al}			Q^0_{2Al}			Q^0_{3Al}			Q^0_{4Al}			
x	δ_{cs} (ppm)	RA (%)	M_2^{Na-P} (10^6rad^2/s^2)	δ_{cs} (ppm)	RA (%)	M_2^{Na-P} (10^6rad^2/s^2)	δ_{cs} (ppm)	RA (%)	M_2^{Na-P} (10^6rad^2/s^2)	δ_{cs} (ppm)	RA (%)	M_2^{Na-P} (10^6rad^2/s^2)	CN_{POAl}
0.1							−16.7	31	4.1	−25.4	69	2.2	3.7
0.20				−2.3	1		−14.9	48	12.7	−24.7	51	6.2	3.6
0.33	5.8	3		−2.8	16	34.3	−12.5	75	16.3	−23.2	5		2.8
0.5	7.3	8	67.8	−2.3	55	45.2	−9.3	37	21.5				2.3

[a] For each glass the average number of P−O−Al bonds per phosphorus, CN_{POAl}, as derived from this phosphorus speciation, is also given. The errors for parameters δ_{cs} and RA were less than ±0.3 ppm, and ±3%, respectively. Typical errors for the M_2 values are ±10%

TABLE 4: ^{31}P Isotropic Chemical Shifts (δ_{cs}), Assignments (Q^n_{mAl}), and Relative Areas (RA) of the Resolvable Signal Components in xNaAlO$_2$−(1 − x)NaPO$_3$ Glasses[a]

		Q^2_{0Al}		Q^1_{2Al}		Q^1_{1Al}		Q^1_{0Al}		Q^0_{1Al}		Q^0_{2Al}		Q^0_{3Al}		
glass		δ_{cs} (ppm)	RA (%)	δ_{cs} (ppm)	RA (%)	δ_{cs} (ppm)	RA (%)	δ_{cs} (ppm)	RA (%)	δ_{cs} (ppm)	RA (%)	δ_{cs} (ppm)	RA (%)	δ_{cs} (ppm)	RA (%)	CN_{POAl}
50−0−50	M	−20.1	100													0
50−5−45	M	−18.0	55	−12.1	8	−6.5	27	1.4	11							0.43
50−7.5−42.5	M	−18.6	19	−12.7	40	−6.1	29	1.4	12							1.1
50−10−40	S			−11.9	57	−5.5	36	1.4	7							1.5
	M			−11.7	56	−5.5	36	1.5	8							1.5
50−12.5−37.5	S[b]			−11.1	43	−4.6	42	1.6	12	6.3	3					1.3
	M			−10.9	42	−4.5	43	1.6	11	6.2	4					1.3
50−16.7−33.4	S									6.5	16	−2.0	54	−8.9	28	2.1
50−20−30	S									6.6	7	−1.4	61	−8.2	32	2.3
50−25−25	S									7.3	8.0	−2.3	55	−9.3	37	2.3

[a] For each glass the average number of P−O−Al bonds per phosphorus, as derived from this phosphorus speciation, is also given. The errors for parameters δ_{cs} and RA were less than ±0.3 ppm and ±3%, respectively. [b] M_2^{Na-P} values are 58, 39, and 18 × 10^6 rad^2/s^2 for Q^1_0 (+Q^0_1), Q^1_1, and Q^1_2 (and/or Q^0_3), respectively.

supported by the ^{27}Al ↔ ^{31}P dipolar NMR measurements along the same lines as reported previously by us for some compositions[4] (see Figure 7 for a new example). All of the ^{27}Al NMR spectra indicate that in general four-, five-, and six-coordinated aluminum sites are present simultaneously at nearly all compositions. Table 2 lists the corresponding ^{27}Al isotropic chemical shifts (δ_{cs}), the ^{27}Al nuclear electric quadrupolar coupling parameters $P_Q = C_Q(1 + \eta^2/3)^{1/2}$ (obtained from ^{27}Al TQMAS experiments), estimated relative peak areas (RA) of each Al site determined by Gauss−Lorentz fits or peak integrations (these values should be considered only approximate because the peaks are slightly asymmetric due to second-order quadrupolar perturbations), and second moment values $M_2(^{27}Al\{^{31}P\})$ specifying the magnitude of the ^{31}P dipolar field at the resolved aluminum sites. Many of the ^{31}P NMR spectra are not resolvable into individual spectral components, and isotropic chemical shifts listed in Table 2 refer to the centers of gravity. For glasses of series II and III in particular, however, reasonable deconvolutions of the ^{31}P NMR line shapes into individual components could be obtained. Tables 3 and 4 list the corresponding peak assignments, the isotropic chemical shifts δ_{cs}, and the relative peak areas. From these assignments, we can estimate the average number of P−O−Al linkages per phosphorus unit, CN_{POAl}, and these numbers are also listed. In large parts, the ^{31}P NMR peak assignments could be supported further by site-resolved double-resonance experiments. For example, Figure 8, left, shows the ^{31}P MAS NMR spectra of three glasses of composition line III, which can be assigned on the basis of site-resolved $^{31}P\{^{27}Al\}$ REAPDOR data. As illustrated on the right part of the figure for the {50−12.5−37.5} glass, the signal component near 1.6 ppm reflects Q^1_{0Al} units, based on the virtual absence of a REAPDOR effect. The peak near −4.5 ppm is most reasonably assigned to Q^0_{2Al} units, while the stronger REAPDOR effect observed for the resonance at −11 ppm suggests a large contribution from Q^0_{3Al} groups (in addition to some Q^1_{2Al} units). Figure 8 illustrates further that the results are virtually identical for melt-cooled and gel-annealed samples. Additional site assignments could be obtained from $^{31}P\{^{23}Na\}$ REDOR studies (see Figures 9 and 10), which were analyzed according to the procedure described in the Methodology Section. Owing to the severely overlapped ^{31}P spectra, for many glasses the data could only be analyzed in terms of an average magnitude of the heteronuclear dipolar field produced by ^{23}Na at the phosphorus nuclei. (For these cases the individual $\Delta S/S_0$ values comprising the REDOR curves were obtained from the integrals over the entire line shape) These results are summarized in Table 5, which also includes the experimental C_Q (^{23}Na) values and the correction factors, f_1, derived from them by SIMPSON simulations, assuming an arbitrarily chosen η value of 0.5. Figure 9 shows representative results obtained for the four glass series investigated. For some glasses of series II and III, site-resolved $^{31}P\{^{23}Na\}$ REDOR data were available from peak deconvolutions (see Figure 10), and the corresponding $M_2(^{31}P\{^{23}Na\})$ values have been included in Tables 3 and 4, respectively. For a given type of site, relatively consistent M_2 values are obtained at different glass compositions. Finally, Figure 11 gives an account of the $^{23}Na\{^{31}P\}$ REDOR experiments conducted; Table 5 illustrates that the measured $M_2(^{23}Na\{^{31}P\})$ values extracted from these data show little variation over a wide range of different glass compositions studied.

I. AlPO$_4$−NaPO$_3$ Glasses. Compared with the conventional melt-cooling method in which the Al_2O_3 content is generally limited to 15 mol %, the present sol−gel route permits the glass preparation along the entire composition line. As seen from Figure 3-left, the ^{27}Al chemical shifts indicate that the local environments of each Al site in all glasses of this series are

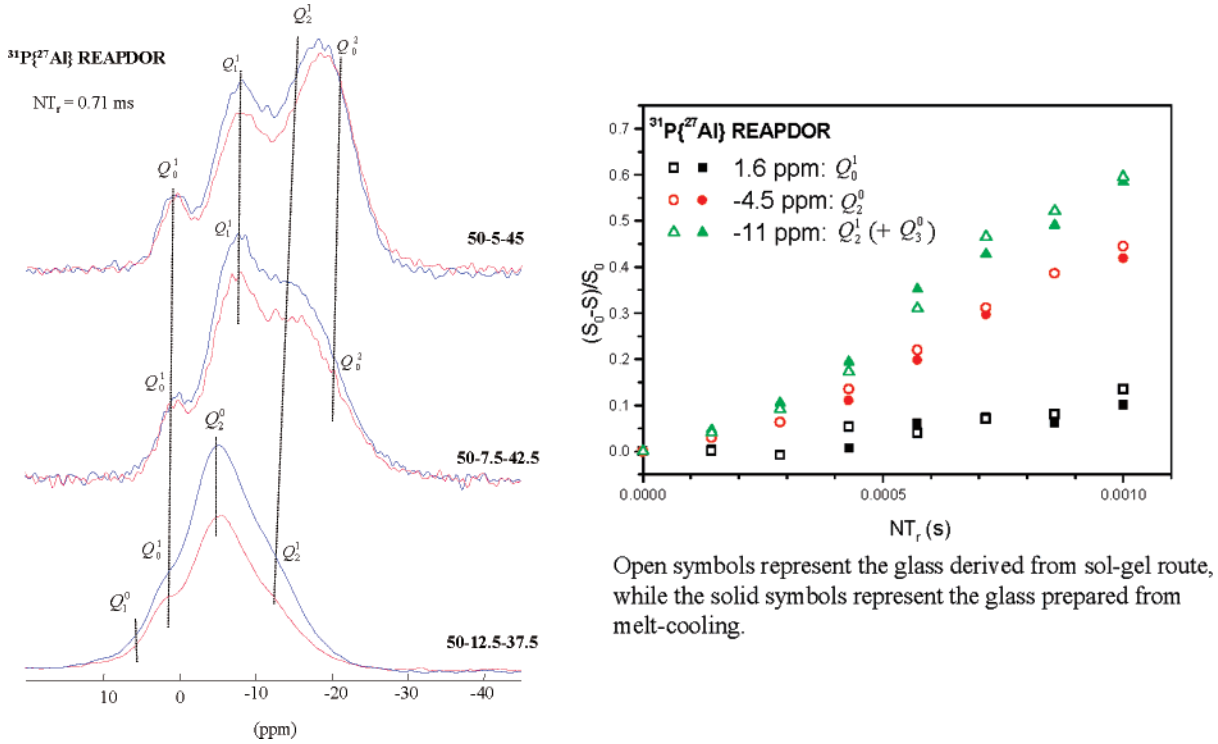

Figure 8. $^{31}P\{^{27}Al\}$ REAPDOR of $xNa_2O-(1-x)AlPO_4$ glasses. Left: comparisons of spectra with and without ^{27}Al irradiation at a dipolar evolution time (NT_r) of 0.71 ms, suggesting the spectral assignments. Right: Site-resolved $^{31}P\{^{27}Al\}$ REAPDOR curves of $50Na_2O-12.5Al_2O_3-37.5P_2O_5$ glasses. The DMFIT software package was used in these spectral deconvolutions.[42] Open symbols represent the glass derived from sol−gel route, while the filled symbols represent the glass prepared from melt-cooling.

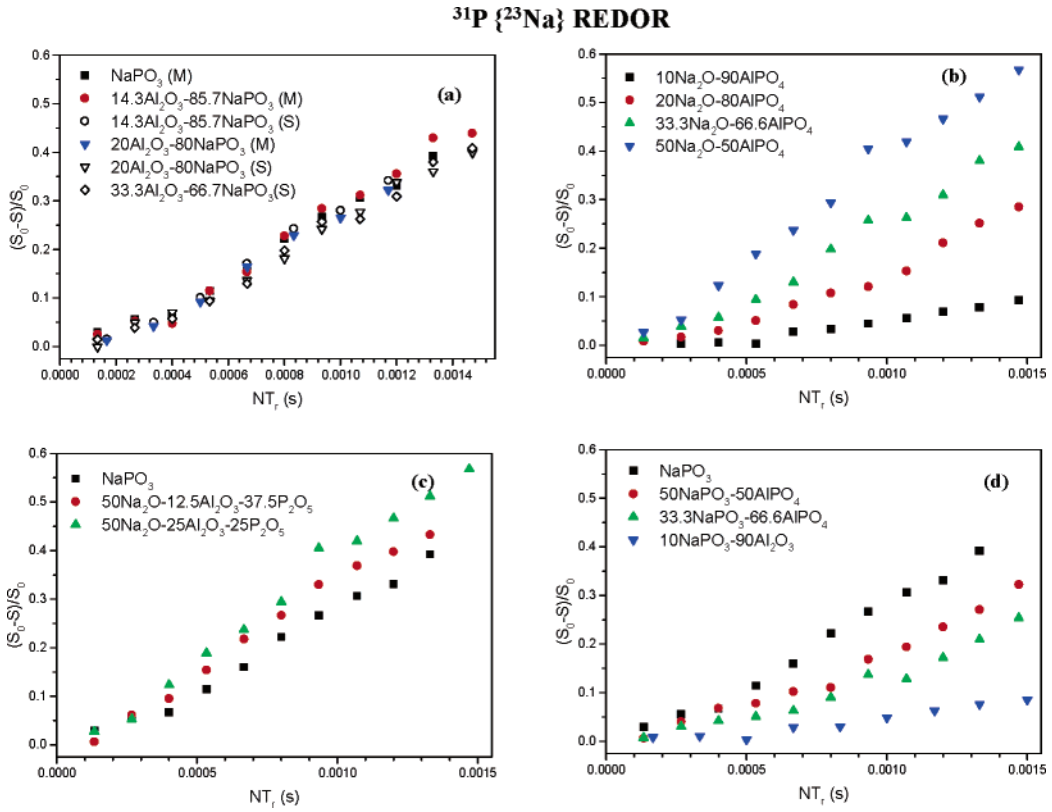

Figure 9. $^{31}P\{^{23}Na\}$ REDOR dephasing curves of sodium aluminophosphate glasses, (a) $Al_2O_3-NaPO_3$ glasses, (b) $Na_2O-AlPO_4$ glasses, (c) $NaAlO_2-NaPO_3$ glasses, and (d) $AlPO_4-NaPO_3$ glasses. The ΔS and S_0 values yielding the $^{31}P\{^{23}Na\}$ REDOR curves are derived from the integrals over the entire ^{31}P spectra, reflecting the average magnitude of the ^{23}Na dipolar field at the ^{31}P nuclei.

completely dominated by phosphorus units (i.e., $Al(OP)_4$, $Al(OP)_5$, and $Al(OP)_6$ units), which is further supported by the M_2 values extracted from the $^{27}Al\{^{31}P\}$ REDOR experiments. Introduction of small amounts of $AlPO_4$ into $NaPO_3$ glass results in a structure dominated by $Al(OP)_6$ units, up to the glass containing 50 mol % $AlPO_4$ (the {25−25−50} composition, which corresponds to the nominal stoichiometry $NaAlP_2O_7$). For this particular composition a crystalline compound is known,

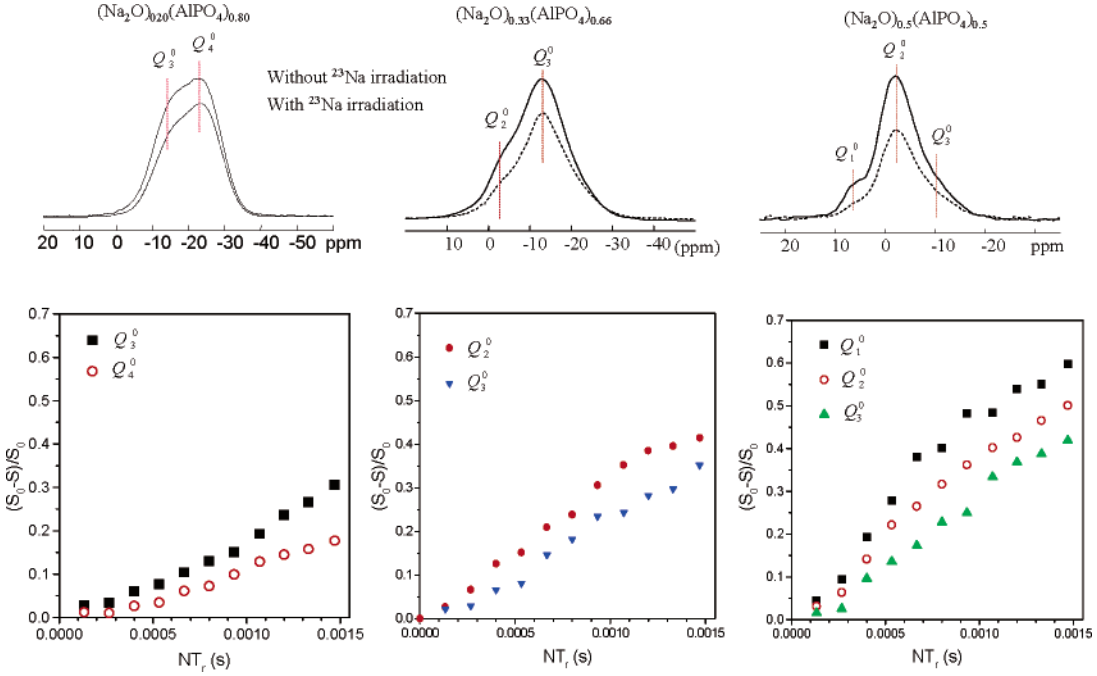

Figure 10. ^{31}P{^{23}Na} REDOR data and site-resolved dephasing curves for xNa$_2$O−(1 − x)AlPO$_4$ glasses: (a) 20Na$_2$O−80AlPO$_4$; (b) 33.3Na$_2$O−66.6AlPO$_4$; (c) 50Na$_2$O−50AlPO$_4$. Spectral deconvolutions were carried out using the DMFIT software package.[42]

TABLE 5: ^{23}Na Isotropic Chemical Shifts (δ_{cs}) and P_Q Values Obtained from ^{23}Na TQMAS, M_2(^{31}P{^{23}Na}) Values, Measured on Selected Glasses, Prepared via Both Sol−Gel (400−500 °C) and Melt-Cooling (1100−1500 °C) Routes[a]

glass $Na_2O_3-Al_2O_3-P_2O_5$		δ_{cs} (ppm)	P_Q (MHz)	f_1	M_2(^{31}P{^{23}Na}) (10^6rad^2/s^2)	M_2(^{23}Na{^{31}P}) (10^6rad^2/s^2)
10−40−50	S	−4.4	2.0	0.0408	2.7	
17−33−50	S	−4.2	2.1	0.0386	7.4	3.1
25−25−50	S	−3.9	2.1	0.0386	11.2	3.5
50−0−50	M	−3.0	2.3	0.0324	24.1	3.3
50−12.5−37.5	S	−1.8	2.2	0.0391	32.4	3.9
50−25−25	S	−1.1	2.3	0.0374	42.0	3.2
33−33−33	S	−1.6	2.3	0.0339	19.9	3.1
20−40−40	S	−2.8	2.1	0.0369	8.9	3.2
10−45−45	S	−2.4	2.2	0.0371	2.5	3.3
43.9−14.3−43.9	S	−1.5	2.4	0.0357	21.7	3.8
	M	−1.8	2.1	0.0409	22.5	4.0
40−20−40	S	−1.3	2.2	0.0361	21.1	3.6
	M	−1.6	2.0	0.0428	21.8	3.9

[a] The errors for parameters δ_{cs}, P_Q, and f_1 were less than ±0.3 ppm, ±0.1 MHz, and ±0.0005, respectively. Typical errors for the M_2 values are ±10%.

the structure of which consists of Q^1_{3Al} pyrophosphate units that are linked by octahedral aluminum and sodium ions.[2,37] All of the spectroscopic evidence obtained in the present study indicates that the structure of the glassy material is organized in a similar fashion. In particular, the relatively small M_2(^{31}P{^{23}Na}) value measured for this glass suggests that the local phosphorus environment is dominated by aluminum, rather than sodium at this composition. On the basis of these considerations, we assign the peak maximum at −21 ppm in the ^{31}P spectra to dominant Q^1_{3Al} units linked mainly by octahedral aluminum. Note that the chemical shift of these units is essentially indistinguishable from that of the Q^2_{0Al} units, resulting in completely unresolved ^{31}P NMR spectra. Owing to this circumstance, the ^{31}P{^{23}Na} REDOR experiments have special assignment significance here.

Upon increasing the AlPO$_4$ content beyond the {25−25−50} composition, the ^{27}Al spectra signify a profound structural transition from six- to four-coordinated aluminum indicating the abrupt formation of Al(OP)$_4$ units. At the same time, the ^{31}P resonance gradually shifts toward −26 ppm, while M_2(^{31}P{^{23}Na}) keeps decreasing linearly toward zero. Both of the latter

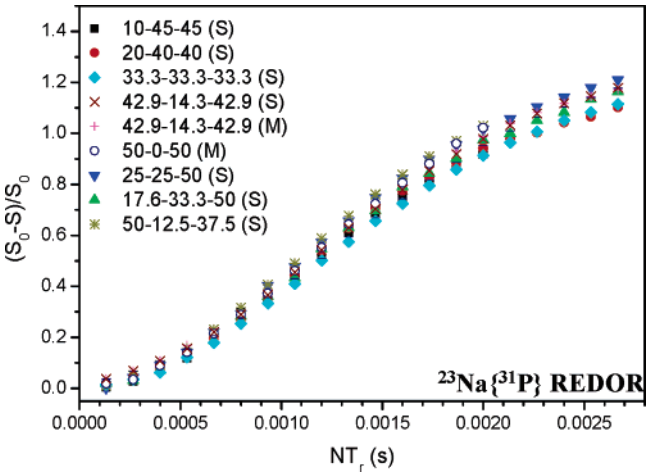

Figure 11. ^{23}Na{^{31}P} REDOR dephasing curves of some representative sodium aluminophosphate glasses.

observations are consistent with the successive appearance of P(OAl)$_4$ units. Finally, the spectra of the AlPO$_4$ end-member

indicate that this glass possesses a silica-like polymeric structure based on alternating $Al(OP)_4$ and $P(OAl)_4$ tetrahedra.[38] Overall, the structural evolution observed along this compositional line can be described by the following sequence:

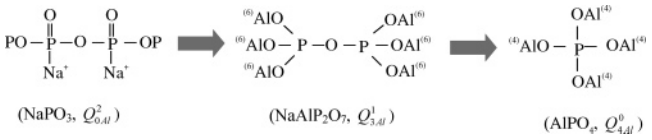

The proposed reaction sequence: $Q^0_{4Al} + Q^2_{0Al} \rightarrow Q^1_{mAl}$ ($0 \leq m \leq 4$, depending on Al content) reflects an equalization of the number of POAl, POP, and PO^-Na^+ bonds between the respective end-members. Obviously, the Q^1_{3Al} unit should be considered a major, but not the exclusive, unit formed at intermediate compositions; we expect that Q^1_{1Al} and Q^1_{2Al} sites may contribute to the structural speciation at lower alumina contents. (Indeed, the shoulder at −10 ppm in the {41.7−8.3−50} glass very likely arises from such units). Furthermore, we cannot exclude the possibility that some amounts of Q^0_{3Al} units contribute to the structure at higher alumina contents. Unfortunately, chemical shift measurements may not be the most reliable guide here because for each of the units mentioned the ^{31}P chemical shift may be subject to some variation, depending on the type of aluminum species (four-, five-, or six-coordinate) they are bonded to.

II. $Na_2O-AlPO_4$ Glasses. None of the glasses along the compositional line $Na_2O-AlPO_4$ can be prepared by melt-cooling.[2,39] The structural conversion observed in the sol−gel prepared glasses as a function of modifier content is illustrated in Figure 4. Introduction of Na_2O into silica-like $AlPO_4$ glass results in the appearance of five- and six-coordinate aluminum, the concentrations of which increase with increasing Na_2O content. The gradual high-frequency shifts of these ^{27}Al resonances, which are observed concomitantly, indicate the successively weakened interaction between aluminum and phosphorus with increasing Na_2O concentration, which is further supported by the $^{27}Al\{^{31}P\}$ REDOR results measured on these glasses (see Table 2). In contrast, the remaining Al(IV) units in these glasses stay fully connected to phosphorus. Successive introduction of Na_2O into $AlPO_4$ glass also has a pronounced effect on the ^{31}P signals: the center of gravity is shifted significantly toward high frequency (see Table 2), reflecting the gradual replacement of POAl bonds by PO^-Na^+ bonds. In the glasses with Na_2O contents lower than 15 mol %, the ^{31}P spectra are dominated by the Q^0_{4Al} resonance at −26 ppm and gradually develop a shoulder near −10 to −15 ppm, which is assigned to Q^0_{3Al} sites. Additional Na_2O modifies the glass further, resulting in the successive appearance of Q^0_{2Al} (−2 to −4 ppm), and Q^0_{1Al} species (7 ppm). Thus, the spectrum of the {33.3−33.3−33.3} glass is dominated by the Q^0_{3Al} resonance, while in the {50−25−25} glass the major unit is Q^0_{2Al}. We note that our assignment suggested here differs from the preliminary site assignment proposed by us in ref 16 and is now fully consistent with the chemical shift assignments made in ref 13 for a different compositional series. Note that the $M_2(^{31}P\{^{23}Na\})$ values are very small for the Q^0_{4Al} sites, which do not have sodium ions nearby, while the magnitude of the ^{23}Na dipolar fields present at the ^{31}P nuclei increases dramatically as the number of nonbridging O atoms increases. This finding parallels that observed in previous studies of silicate glasses[40] and binary sodium (lithium) phosphate glasses.[22,41] Altogether these NMR data confirm that the polymerized phosphorus species of pure glassy $AlPO_4$ are successively depolymerized with increasing Na_2O content, resulting in a structural evolution along the sequence $Q^0_{4Al} \rightarrow Q^0_{3Al} \rightarrow Q^0_{2Al} \rightarrow Q^0_{1Al}$. At the same time, the $Al(OP)_4$ sites are converted to higher-coordinated aluminum units that are only weakly connected to phosphorus.

III. $NaAlO_2-NaPO_3$ Glasses. Glasses along this composition line (with alumina contents up to 17.5 mol %) have been studied previously by Lang et al., who also contributed some qualitative data from $^{31}P\{^{27}Al\}$ and $^{31}P\{^{23}Na\}$ TRAPDOR NMR.[13] Figure 5 shows our own results over the more extended composition range available by sol−gel synthesis. In agreement with ref 13 we find that in glasses with low alumina contents the dominant mode of aluminum bonding is the formation of octahedral $Al(OP)_6$ units (Figure 5b, d, and f). Upon increasing the $NaAlO_2$ content up to 16.7 mol %, the six-coordinated units are successively displaced by tetrahedral $Al(OP)_4$ groups (see Figure 5f, j, and n), which become the nearly exclusive aluminum species in the {50−16.7−33.3} glass. Our ^{31}P NMR spectra are largely consistent with those reported in ref 13. Figure 5-right illustrates that the introduction of $NaAlO_2$ into $NaPO_3$ glass alters the structure dramatically. In the {50−10−40} glass, three local environments can be identified: the components near 1.4 and −5.5 ppm can be assigned to Q^1_{0Al} and Q^1_{1Al} units, respectively. Considering the number of P−O−Al bonds extracted from an analysis of the ^{27}Al NMR spectra, the resonance near −12 ppm is most likely attributable to Q^1_{2Al} units. For the {50−16.7−33.3} glass, the ^{27}Al NMR spectrum suggests a particularly simple structure: nearly all of the aluminum is present as $Al(OP)_4$ units. From the balance of P−O−Al linkages we must then conclude that the P atoms have (on average) two linkages to aluminum. This expectation agrees very well with the dominant ^{31}P resonance found at −2.0 ppm. As the {50−16.7−33.3} glass lies halfway along the $Na_3PO_4-AlPO_4$ line in the composition diagram, its structural speciation can thus roughly be viewed to reflect the "melt reaction" $Q^0_{0Al} + Q^0_{4Al} \rightarrow 2\ Q^0_{2Al}$. Naturally, some disorder is present, resulting in some minor ^{31}P NMR peaks that are attributable to Q^0_{1Al} and Q^0_{3Al} sites (6.5 and −8.9 ppm, respectively; and the latter signal component might contain an additional contribution from Q^1_{2Al} sites). Altogether, the structural evolution of phosphorus of this glass series with increasing the alumina content can be viewed in terms of the gradual transition $Q^2_{0Al} \rightarrow Q^1_{mAl} \rightarrow Q^0_{mAl}$.

Upon increasing the alumina concentration beyond 16.7 mol %, (Figure 5p and r), new Al(V) and Al(VI) environments appear, the chemical shifts of which suggest a lower degree of Al−O−P connectivity. This result is confirmed by the $^{27}Al\{^{31}P\}$ REDOR results (Table 2). The ^{31}P NMR signals remain nearly unchanged, however, indicating that the phosphorus speciation remains nearly constant at these compositions. All of these results suggest that the alumina component is partially segregated in these glasses.

IV. $Al_2O_3-NaPO_3$ Glasses. A detailed NMR account of this composition line (prepared by sol−gel synthesis) has been published previously by us in ref 5; however, for completeness, the MAS NMR results are included in Figure 6. The dominant aluminum coordination changes from six to four at 14.3 mol % Al_2O_3. Upon increasing the Al_2O_3 content up to 25 mol %, $Al(OP)_4$ units become the dominant aluminum environment. Further addition of Al_2O_3 (e.g., up to 33 mol %) results in increased concentrations of Al(V) and Al(VI) environments; however, the concomitant high-frequency shifts and the $^{27}Al\{^{31}P\}$REDOR results indicate these units to have low P−O−Al connectivity. The ^{31}P spectra are poorly resolved and signify

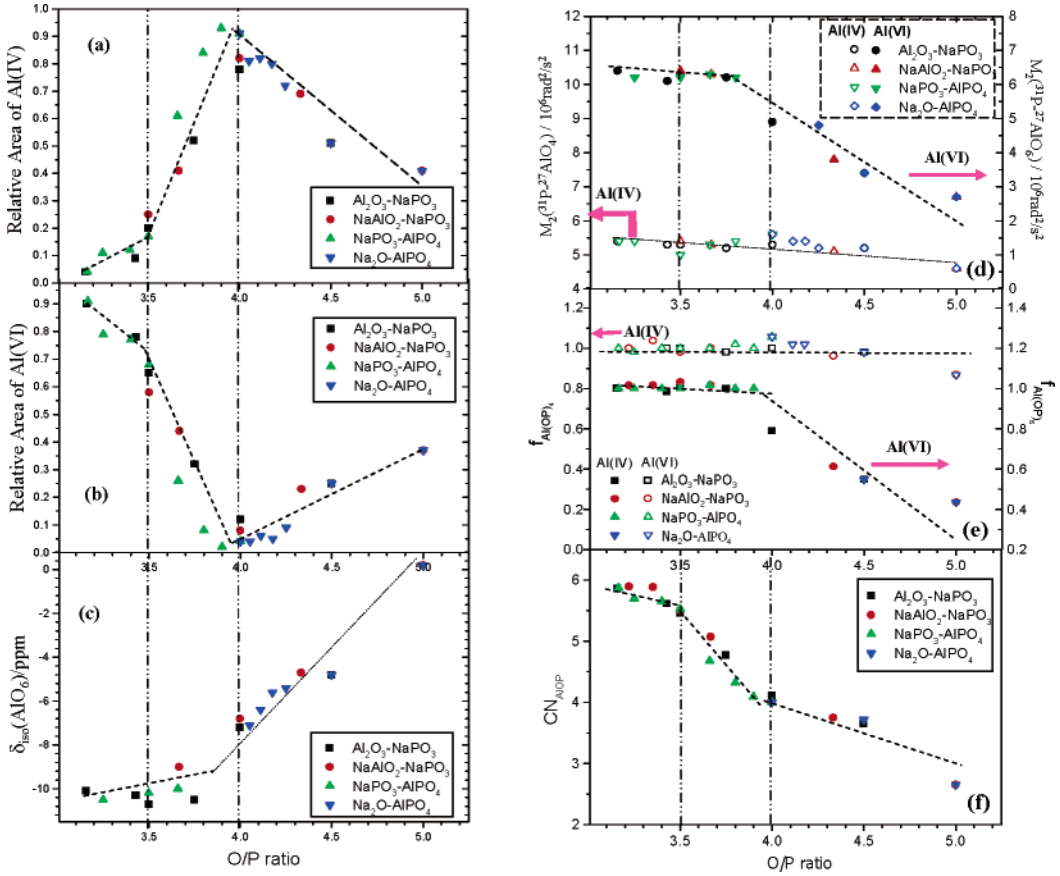

Figure 12. Dependence of short- and medium-range order parameters in sodium aluminophosphate glasses on the O/P ratio: (a and b) relative area of Al(IV) (a) and Al(VI) (b) units, (c) isotropic chemical shift, δ_{CS}(Al(VI)), of the octahedral aluminum units, (d) $M_2(^{27}Al\{^{31}P\})$, (e) fraction f_{AlOP} of aluminum−oxygen bonds that are linking to phosphorus, for Al(IV) and Al(VI), respectively, and (f) average number CN_{AlOP} of Al−O−P bonds per aluminum atom.

the formation of Q^1_{mAl} and Q^0_{mAl} groups ($m = 1, 2$). At alumina contents of up to 25 mol % and higher, the balance of P−O−Al units suggests that the majority of the phosphorus species are of the Q^0_{mAl} type. Interestingly, the $^{31}P\{^{23}Na\}$ REDOR data suggest that the extent of these heterodipolar interactions is rather independent of alumina content. This result indicates that the main compositional effect in this glass system is the successive replacement of P−O−P− by P−O−Al bonding, leaving the extent of cation binding by the anionic phosphate groups essentially unaltered. Thus, all of the experimental evidences indicate that the main structural transformation occurring along this compositional line is best described by the sequence $Q^2_{0Al} \rightarrow (Q^1_{1Al} + Q^1_{2Al}) \rightarrow (Q^0_{2Al} + Q^0_{3Al})$. In glasses with alumina contents beyond 25 mol %, the extent of P−O−Al connectivity is diminished again.

5. Discussion

Previous results have shown that the physical properties of sodium aluminophosphate glasses are critically influenced by the O/P ratio, reflecting the metaphosphate (O/P = 3.0) → pyrophosphate (O/P = 3.5) → orthophosphate (O/P = 4.0) structural transition.[2] It has been noted further that the local aluminum environments of various compositional lines change dramatically in the region 3.5 < O/P < 4.0, indicating an abrupt change from six- to four-coordination.[9] Results from the four compositional lines measured within the frame of the present study indicate that the O/P ratio affects both the local and the medium range order in these glasses in a universal manner for the entire system. For all of the glasses with O/P < 3.5, the ^{27}Al NMR spectra indicate that the octahedral Al(OP)$_6$ units overwhelmingly dominate the local structures. The pyrophosphate composition (O/P = 3.5), corresponding to $x = 0.5$, 0.11, and 0.14 for lines I, III, and IV, respectively, marks the onset of abrupt structural change: the concentration of Al(IV) increases dramatically at the expense of Al(VI) units for all series of glasses (Figures 3−6). At the orthophosphate composition (O/P = 4), corresponding to $x = 1$, 0, 0.2, and 0.25, for lines I, II, III, and IV, respectively, tetrahedral Al(OP)$_4$ units become the overwhelmingly dominant aluminum environment. Finally, at glass compositions with O/P ratios > 4.0 (only accessible via sol−gel synthesis) the concentrations of Al(VI) and Al(V) increase again, while high-frequency shifts of their resonance signals as well as significantly reduced $M_2(^{27}Al\{^{31}P\})$ values indicate that these species are only weakly connected with phosphorus. Figure 12a−c reveals that the relative areas of the Al(IV) and Al(VI) units, as well as the ^{27}Al isotropic chemical shifts of the octahedral aluminum species (δ_{cs}(Al(VI))) derived from TQMAS, are universally correlated with the O/P ratio for all four series of glasses investigated here.

Analogous universality is observed in the medium-range order. Figure 12d plots the dependence of $M_2(^{27}Al\{^{31}P\})$ on O/P ratio, both for the Al(IV) and Al(VI) units in all of the glasses of the present study. For the Al(IV) units, nearly constant M_2 values are observed over the entire glass-forming range, indicating that the Al(IV) environments always remain fully connected with phosphorus ligands. For the Al(VI) units the values remain nearly constant at O/P ratios < 4, and decrease significantly at higher O/P; this effect is directly correlated with the high-frequency shifts of the ^{27}Al(VI) signals (Figure 12c)

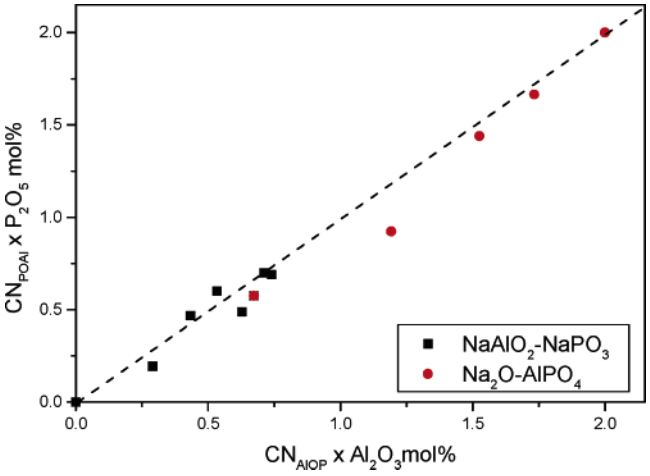

Figure 13. Consistency check regarding P−O−Al connectivity information from NMR: The total number of Al−O−P bonds (CN_{AlOP} × Al_2O_3 mol %) derived from ^{27}Al NMR is plotted vs the total number P−O−Al bonds (CN_{POAl} × P_2O_5 mol %) derived from ^{31}P NMR. Included are all those glasses for which unambiguous ^{31}P NMR peak assignments were obtained.

as discussed above. For the Al(V) units essentially the same behavior is observed (data not shown). Figure 12e shows the fraction $f_{Al(OP)n}$ ($n = 4,5,6$) of those aluminum−oxygen linkages that are bonded to phosphorus (assuming exclusive corner-sharing). This parameter remains close to 1.0 in all of the glasses with O/P ratios up to 4.0. Beyond, $f_{Al(OP)4}$ remains constant near 1.0, whereas $f_{Al(OP)5}$ and $f_{Al(OP)6}$ decrease substantially, signifying the onset of Al−O−Al bonding.

Using the above M_2 data we can quantify the average number of Al−O−P bonds per Al atom (CN_{AlOP}) from the relative areas (*RA*) and the second moment ($M_2(^{27}Al\{^{31}P\})$ values measured for each ^{27}Al MAS NMR peak:

$$CN_{AlOP} = 4 \times RA(IV) \times M_2(^{27}Al\{^{31}P\},AlO_4)/5.3 + 5 \times RA(V) \times M_2(^{27}Al\{^{31}P\},AlO_5)/6.0 + 6 \times RA(VI) \times M_2(^{27}Al\{^{31}P\},AlO_6)/6.2 \quad (4)$$

Here, the M_2 values are given in units of 10^6 rad^2/s^2 and the denominator values 5.3, 6.0, and 6.2 (also in units of 10^6 rad^2/s^2) are the average experimental M_2 values for fully connected $Al(OP)_4$, $Al(OP)_5$, and $Al(OP)_6$ environments, respectively, as measured on samples with low Al/P ratios. Equation 4 implies that the M_2 values scale linearly with the number of Al−O−P linkages; this is true provided no large variations in the corresponding internuclear distances occur. Figure 12f summarizes the dependence of CN_{AlOP} on the O/P ratio, again revealing universal behavior for all four composition lines studied. The dramatic structural transition observed within the region 3.5 < O/P < 4.0 and the onset of Al−O−Al bonding are also evidenced by this parameter. We note that CN_{AlOP}, the average number of Al−O−P links per aluminum site as estimated by the above procedure, is found to be nicely consistent with CN_{POAl}, the average number of P−O−Al links as extracted from the deconvolution (where possible) of the ^{31}P NMR spectra. This is illustrated in Figure 13, in which both parameters (each weighted by the molar percentages of the phosphorus and alumina components) are plotted against each other.

A further aspect of medium range order concerns the network former/network modifier correlations evidenced by the quantitative $^{31}P\{^{23}Na\}$ REDOR data obtained in the present study. As

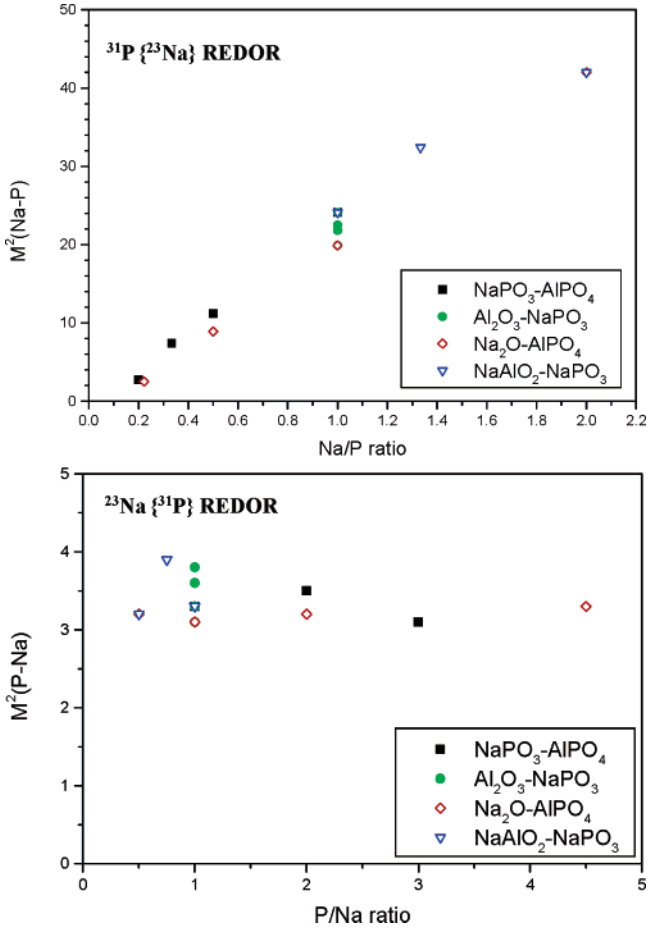

Figure 14. Dependences of $M_2(^{31}P\{^{23}Na\})$ on Na/P ratio (top) and of $M_2(^{23}Na\{^{31}P\})$ on P/Na ratio (bottom).

indicated by Figure 9a the average ^{23}Na dipolar field at the ^{31}P sites is almost unaffected by the alumina concentration in Al_2O_3−$NaPO_3$ glasses, where the P/Na ratio remains fixed at 1.0. In contrast, strong composition dependences are observed for glasses along each of the other three series (Figure 9b−d). Figure 14a indicates that the $M_2(^{31}P\{^{23}Na\})$ values in this glass system are universally correlated with the Na/P ratios, suggesting that the sodium introduced into the aluminophosphate glass-network is located mostly around phosphorus (not aluminum) units. This view is further supported by $^{23}Na\{^{31}P\}$ REDOR measurements on these glasses (Figure 11), from which the derived $^{23}Na\{^{31}P\}$ dipolar second moments are found essentially independent of the P/Na ratio ranging from 0.5 to 4.5 (see Figure 14b). Evidently, the average number of phosphorus atoms surrounding each sodium atom locally is generally unaffected by the composition, suggesting that the local environment of sodium is dominated mainly by the phosphorus rather than aluminum in all sodium aluminophosphate glasses.

6. Conclusions

The local structure and connectivities of sodium aluminophosphate glasses in a compositional range significantly extended by a sol−gel route were investigated using high-resolution advanced solid-state NMR techniques. Detailed structural speciations for the network former species aluminum and phosphorus were derived from the deconvolution of high-resolution ^{27}Al and ^{31}P NMR spectra and supported by quantitative $^{27}Al\{^{31}P\}$ REDOR and qualitative $^{31}P\{^{27}Al\}$ REAPDOR experiments. The numbers of P−O−Al linkages that could be extracted from either ^{31}P or ^{27}Al NMR were found to be very

consistent with each other; in general, the formation of P−O−Al linkages is greatly favored over P−O−P or Al−O−Al linkages. Results obtained for glass series along four compositional lines reveal that features of local and medium range order are universally correlated with the overall O/P ratio of these glasses. A dramatic decrease in Al−O−P connectivity occurs at glass compositions intermediate between pyrophosphate (O/P = 3.5) and orthophosphate compositions (O/P = 4), which corresponds to a sudden structural transformation from preferred $Al(OP)_6$ units to preferred $Al(OP)_4$ environments. Glasses with even higher O/P ratios are only available by sol−gel preparation techniques. In these glasses, the average extent of Al−O−P connectivity is decreased significantly and new types of five- and six-coordinated aluminum units signify the onset of Al−O−Al bonding; at the same time, sodium phosphate-like environments are formed. While under melt-cooling conditions these processes result in crystallization, the latter are suppressed in the sol−gel derived materials, owing to the significantly lower gel annealing temperatures, resulting in a widely increased glass forming region.

Acknowledgment. Financial support from Deutsche Forschungsgemeinschaft (grant Ec168/4-2) is gratefully acknowledged. We thank Ms. Wilma Pröbsting for the thermoanalytical characterization.

References and Notes

(1) (a) Kreidl, N. J.; Weyl, W. A. *J. Am. Ceram. Soc.* **1941**, *24*, 372. (b) Kumar, S. *Cent. Glass Ceram Res. Inst. Bull* (*India*) **1956**, *2*, 183. (c) Kumar, S. *Cent. Glass Ceram. Res. Inst. Bull.* (*India*) **1960**, *7*, 117.
(2) Brow, R. K. *J. Am. Ceram. Soc.* **1993**, *76*, 913.
(3) Kishioka, A.; Hayashi, M.; Kinishita, M. *Bull. Chem. Soc. Jpn.* **1976**, *49*, 3032.
(4) Zhang, L.; Eckert, H. *Solid State Nucl. Magn. Reson.* **2004**, *26*, 132.
(5) Zhang, L.; Eckert, H. *J. Non-Cryst. Solids*, in press.
(6) Eckert, H. *Prog. NMR Spectrosc.* **1992**, *24*, 159.
(7) Eckert, H. In *Encylopedia of NMR Spectroscopy*; Grant, D., Harris, R. K., Eds.; Wiley-Interscience, 1996.
(8) Eckert, H.; Elbers, S.; Epping, J. D.; Janssen, M.; Kalwei, M.; Strojek, W.; Voigt, U. *Top. Curr. Chem.* **2005**, *246*, 195.
(9) Brow, R. K.; Kirkpatrick, R. J.; Turner, G. L. *J. Am. Ceram. Soc.* **1993**, *76*, 919.
(10) Brow, R. K.; Kirkpatrick, R. J.; Turner, G. L. *J. Am. Ceram. Soc.* **1990**, *73*, 2293.
(11) Kirkpatrick, R. J.; Brow, R. K. *Solid State NMR* **1995**, *5*, 9.
(12) Egan, J. M.; Wenslow, R. M.; Mueller, K. T. *J. Non-Cryst. Solids* **2000**, *261*, 115.
(13) Lang, D. P.;. Alam, T. M.; Bencoe, D. N. *Chem. Mater.* **2001**, *13*, 420; see also references therein.
(14) Schneider, J.; Oliveira, S. L.; Nunes, L. A. O.; Panepucci, H. *J. Am. Ceram. Soc.* **2003**, *86*, 317.
(15) Zhang, L.; Bögershausen, A.; Eckert, H. *J. Am. Ceram. Soc.* **2005**, *88*, 897.
(16) Zhang, L.; Eckert, H.; Helsch, G.; Frischat, G. H. *Z. Phys. Chem.* **2005**, *219*, 71.
(17) Gullion, T.; Schaefer, J. *J. Magn. Reson.* **1989**, *81*, 196.
(18) Gullion, T. *Magn. Reson. Rev.* **1997**, *17*, 83.
(19) Bertmer, M.; Eckert, H. *Solid State Nucl. Magn. Reson.* **1999**, *15*, 139.
(20) Gullion, T. *J. Magn. Reson.* **1995**, *A117*, 326.
(21) Chopin, L.; Vega, S.; Gullion, T. *J. Am. Chem. Soc.* **1998**, *120*, 4406.
(22) Strojek, W.; Kalwei, M.; Eckert, H. *J. Phys. Chem. B* **2004**, *108*, 7061−7073.
(23) Bertmer, M.; Züchner, L.; Chan, J. C. C.; Eckert, H. *J. Phys. Chem. B* **2000**, *104*, 6541.
(24) Zhang, L.; Eckert, H. *J. Mater. Chem.* **2005**, *15*, 1640.
(25) Zhang, L.; de Araujo, C. C.; Eckert, H. *Chem. Mater.* **2005**, *17*, 3101.
(26) Gullion, T. *Concepts Magn. Reson.* **1998**, *10*, 277.
(27) Garbow, J. R.; Gullion, T. *J. Magn. Reson.* **1991**, *95*, 442.
(28) Chan, J. C. C.; Eckert, H. *J. Magn. Reson.* **2000**, *140*, 170.
(29) Schmidt, A.; MacKay, R. A.; Schaefer, J. *J. Magn. Reson.* **1992**, *96*, 644.
(30) Hudalla, C.; Eckert, H.; Dupree, R. *J. Phys. Chem.* **1996**, *100*, 15986.
(31) Bak, M.; Rasmussen, J. T.; Nielsen, N. C. *J. Magn. Reson.* **2000**, *147*, 296.
(32) Ba, Y.; Kao, H. M.; Grey, C. P.; Chopin, L.; Gullion, T. *J. Magn. Reson.* **1998**, *133*, 104.
(33) Medek, A.; Harwood: J. S.; Frydman, L. *J. Am. Chem. Soc.* **1995**, *117*, 12779.
(34) Amoureux, J. P.; Fernandez, C.; Steuernagel, S. *J. Magn. Reson.* **1996**, *A123*, 116.
(35) Züchner, L.; Chan, J. C. C.; Müller-Warmuth, W.; Eckert, H. *J. Phys. Chem. B* **1998**, *120*, 4495.
(36) Ng, H. N.; Calvo, C. *Can. J. Chem.* **1973**, *51*, 2613.
(37) Dietzel, A.; Hinz, I. *Ber. Dtsch. Keram. Ges.* **1962**, *39*, 569.
(38) Dietzel, A. *J. Non-Cryst. Solids* **1985**, *73*, 47.
(39) Voigt, U.; Lammert, H.; Eckert, H.; Heuer, A. *Phys. Rev. B* **2005**, *72*, 064207.
(40) van Wüllen, L.; Schwering, G.; Eckert, H. *Chem. Mater.* **2000**, *12*, 1840.
(41) Strojek, W.; Eckert, H. *Phys. Chem. Chem. Phys.*, in press.
(42) Massiot, D.; Fayon, F.; Capron, M.; King, I.; Le Calvé, S.; Alonso, B.; Durand, J.-O.; Bujoli, B.; Gan, Z.; Hoatson, G. *Magn. Reson. Chem.* **2002**, *40*, 70.